Proceedings of CTD 2020
PROC-CTD2020-59
July 16, 2020

The Track finder algorithm for the trigger system of the Mu2e experiment at Fermilab

D. Brown[1], G. Pezzullo[2†], P. Murat[3]

[1] *Lawrence Berkeley National Laboratory, 1 Cyclotron Rd, Berkeley (CA), USA*
[2] *Department of Physics, Yale University, 217 Prospect St, New Haven (CT), USA*
[3] *Fermi National Accelerator Laboratory, Main Entrance Rd, Batavia (IL), USA*

ABSTRACT

The Mu2e experiment at Fermilab will search for two charged-lepton flavor violating processes: $\mu^- \to e^-$ and $\mu^- \to e^+$ conversions in the field of an aluminum nucleus, improving by four orders of magnitude the search sensitivity reached so far. The signature of the Mu2e signals is represented by a ∼105 MeV/c e^- and a ∼92 MeV/c e^+ in the two channels respectively. The reconstruction and identification of the signal particle tracks in the Mu2e tracker is difficult due to the presence of spurious hits, low-energy Compton e^- and other lower momenta e^- generated in μ Decay-In-Orbit processes, $\mu^-\mathrm{N} \to e^-\mathrm{N}\overline{\nu}_e\nu_\mu$. The Mu2e trigger is based on the online track reconstruction, which exploits two pattern recognition algorithms followed by the fast track fit. Preliminary studies show that the online track reconstruction will deliver a trigger rate of a few hundreds Hz, which includes a rate of fake tracks below ∼10 Hz. The trigger signal efficiency is expected to be larger than 96% w.r.t the offline reconstruction. A prototype of the TDAQ system has been built at Fermilab, and we report on its timing performance.

PRESENTED AT

Connecting the Dots Workshop (CTD 2020)
April 20-30, 2020

†g.pezzullo@yale.edu

1 Introduction

lepton flavor violation (LFV) has been observed in the neutral sector (neutrino oscillations), but not in the charged sector. In the Standard Model, the predicted rate of charged lepton flavor violating (CLFV) processes is below 10^{-50}s [1]. However, many theories beyond the SM predict CLFV processes with rates observable by currently constructed HEP experiments [1]. The Mu2e apparatus includes three superconducting solenoids as shown in Figure 1: (1) the production solenoid, where an 8 GeV proton pulsed-beam (period ∼1.7 μs) hits a tungsten target, producing mostly pions; (2) the transport solenoid, which serves as decay "tunnel" for the pions, and makes also charge and momentum selection, creating a low-momentum μ^- beam; (3) the detector solenoid, which houses an aluminum Stopping Target, where the muons get stopped and form muonic atoms, and the detector system (in a 1T solenoidal magnetic field) optimized to detect electron and positron from the μ conversions. The entire detector solenoid and half of the transport solenoid are covered with a cosmic-ray veto system (CRV), made out of 4-layers of extruded scintillator bars. The detector consists

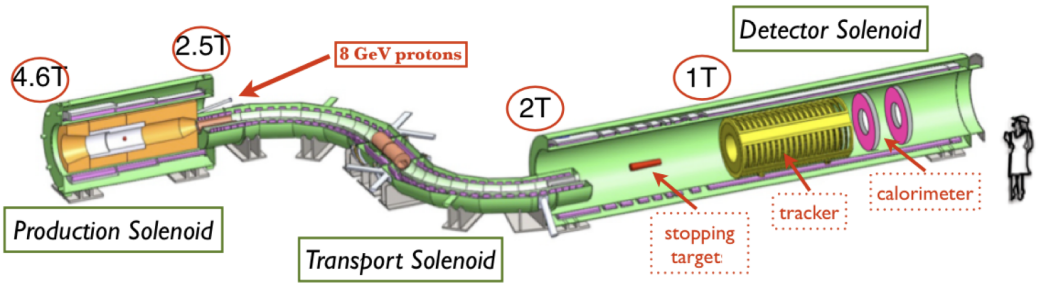

Figure 1: Mu2e experimental apparatus. The cosmic-ray veto system is not shown.

of a 3.2 m long straw tube tracker and a crystal calorimeter. Both the tracker and the calorimeter have cylindrical symmetry. The inner part of each detector has an opening which provides for the free passage of non-interacting beam and makes the detectors "blind" to low-momentum charged background particles produced in the stopping target. The tracker consists of 36 equally spaced tracking planes, made out of 6

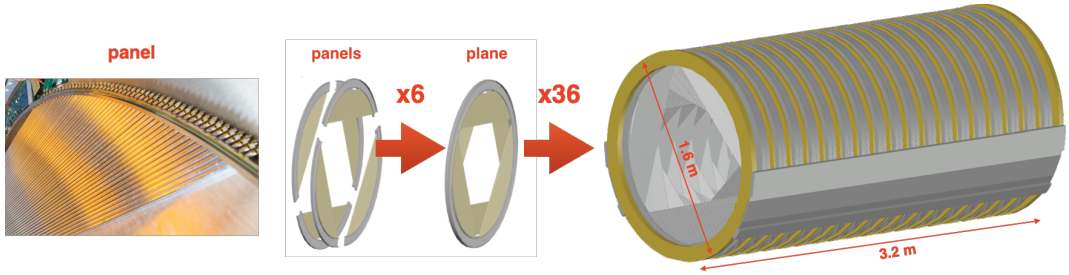

Figure 2: Explosion of the Mu2e tracker.

rotated panels arranged over two faces. A panel represents the basic unit of the tracker; it consists of 2 two staggered layers of straw tubes and has 96 straws in total. A more detailed description of the detector can be found in references: [4, 5]. The coordinate system is right-handed. The Z-axis parallel to the detector solenoid axis and is positively oriented moving from the stopping target to the detector region, with the origin in the middle of the tracker. The Y-axis is normal to the plane where all the three solenoids lay, and is posi- tively oriented in the opposite direction of the ground. Then the X-axis is defined by the vector product of the other two axis: $\vec{x} = \vec{y} \times \vec{z}$.

2 Trigger system architecture

Mu2e uses *artdaq*[9] and *art*[8] software as event filtering and processing frameworks respectively. The detector Read Out Controllers (ROC), from the tracker and calorimeter, stream out continuously the data, zero-suppressed, to the Data Transfer Controller units (DTC). The data of a given event is then grouped in a single server using a 10 GBytes switch. Then, the online reconstruction of the events starts and make a trigger decision. If an event gets triggered, we pull also the data from the CRV and we aggregate them in a single data stream. The trigger system needs to satisfy the following requirements:

1. provide efficiency better than 90% for the signals;
2. keep the trigger rate below a few kHz - equivalent to ~ 7 Pb/year;
3. achieve a processing time < 5 ms/event.

Our main physics triggers use the info of the reconstructed tracks to make the final decision. In the following sections, we describe the logic of the online track reconstruction as well as its expected performance.

3 Online track finder

The first stage of the track search is the hits preparation. The signals at both sides of the straw tubes are combined to reconstruct the hit time as well as the position along the wire. Then, we combine neighboring hits, within the same panel, to create a so-called "panel hit". For a given real track, more than 90% of the panel hits group 2 straw hits. This step allows to improve the spatial resolution along the wire direction (by a factor $\sim \sqrt{2}$) and reduce the combinatorics in the next stages of the reconstruction. After that, we use a Multi-Variate-Analysis (MVA) algorithm to identify and flag as "background" the hits compatible with being produced by a low-momentum (a few MeV) Compton e^- . These flagged hits will be excluded from the pattern-recognition. After the hits preparation, we exploit two separate pattern-recognition methods: a

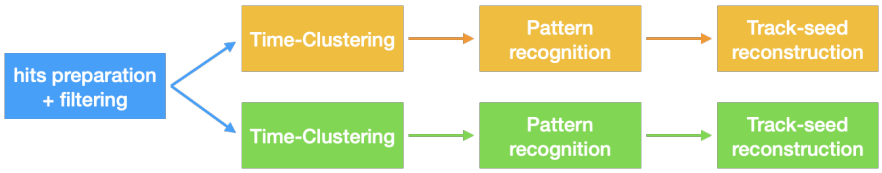

Figure 3: Graph of the online track reconstruction logic.

calorimeter-seeded (calo-seeded) and a tracker-seeded (trk-seeded) algorithm. Figure 3 shows a graph of the logic adopted.

3.1 Tracker-seeded pattern recognition

The pattern recognition proceeds in two steps: the hit time-clustering and the helix reconstruction. The time-clustering uses an MVA-based algorithm to identify peaks in the distribution of the hit time. To improve the accuracy of this procedure, the hit time is extrapolated to z=0 (the middle of the tracker), assuming: (i) a $\beta = v/c = 1$ and (ii) a track pitch angle equal to the average value expected for a conversion electron (CE). This also allows to factorize out the particle time of flight from the width of the peak we are looking for.

The helix reconstruction is divided into two main parts: (i) the circle reconstruction in the transverse plane (XY) and (ii) the line reconstruction in the ϕ-Z plane, where ϕ is the hit polar angle w.r.t. the helix axis, while z is the coordinate along the tracker central axis. The two steps are integrated into an iterative loop that performs a hit-clean up at each iteration to remove eventual outliers. The circle reconstruction starts by looping over all the possible triplets of hits (picked from different tracking faces); if a triplet covers a sufficient area, we evaluate the expected helix center $(x_0,\ y_0)$ from the intersection of the two perpendicular

bisectors. When the loop is ended, the best estimate of $(x_0,\ y_0)$ is extracted by taking the median of all the values collected. Once we have estimated the circle center, a loop is repeated over the hits to estimate the circle radius using again the median of all the single values.

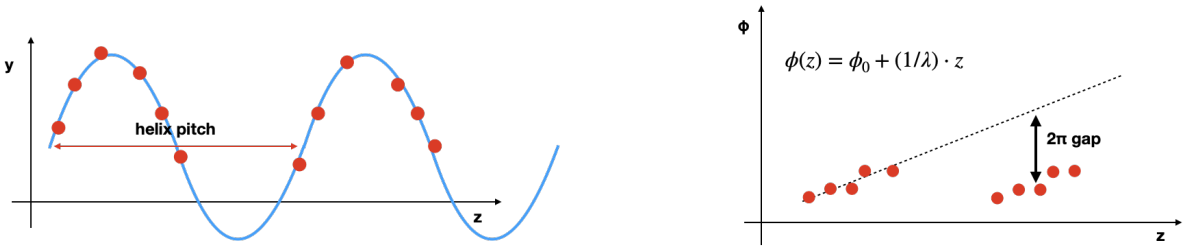

Figure 4: Drawing of a signal helix in the tracker Y-Z longitudinal plane (left) and its projection in the ϕ-Z plane (right).

To perform the ϕ-Z reconstruction we need to resolve the 2π ambiguity of the hits. Figure 4 shows the origin of this problem; a typical signal track reconstructed in our chamber makes multiple loops, but given the presence of the hollow, only arches appear in the longitudinal plane Y-Z and in the plot ϕ vs Z, we see groups of hits for each loop. We need to add a factor $2\pi \cdot i$ to the ϕ of the hits belonging to the i-th loop, but to make this correction we need to know the particle angular velocity $d\phi/dz = 1/\lambda$. The first estimate of $d\phi/dz$ is obtained by making the histogram of $d\phi/dz_{i,j,k} = \frac{(\phi_j + 2\pi k) - \phi_i}{z_j - z_i}$, with $i, j \in (0, \mathrm{N}-1)$ and $k \in (0, 10)$. The peak of the resulting distribution is used to assign each hit to the corresponding loop and thus resolve the 2π ambiguity. This allows us to create the histogram of $d\phi/dz_{i,j} = \frac{\phi_j - \phi_i}{z_j - z_i}$, whose peak is used as best estimate of the helix $d\phi/dz$. Figure 5 shows the distributions of the reconstructed momentum and

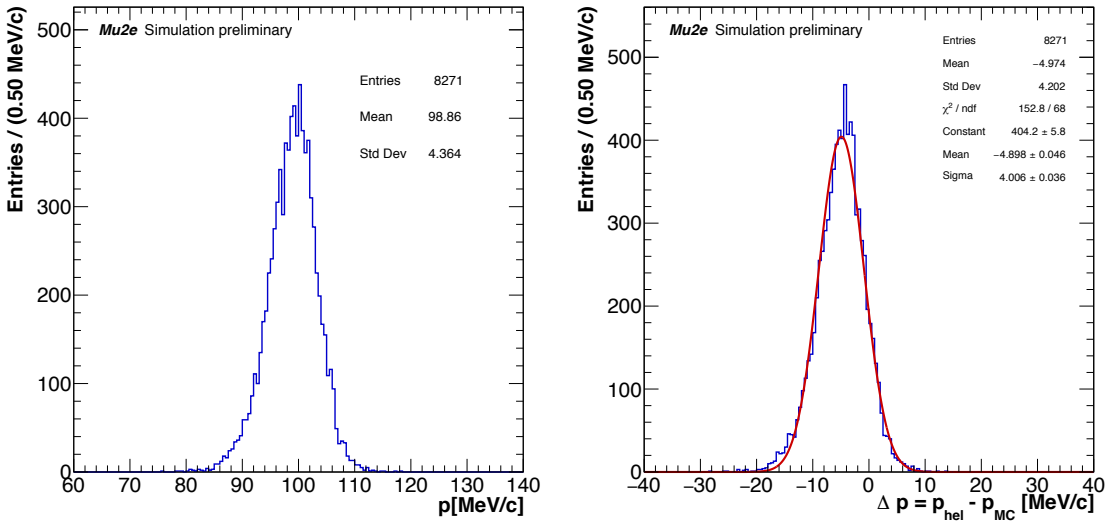

Figure 5: Distribution of the reconstructed momentum (left) and of the momentum resolution (right) for the tracker-seeded algorithm. Results were obtained processing a MC sample of CE overlaid with the expected background.

the expected momentum resolution. The distributions were obtained by processing a dataset of CE overlaid with the expected background sources. A Gaussian fit to the distribution of the momentum residuals shows that the expected resolution for a CE is $\sim 4\%$. The non-zero mean of the Gaussian fit is due to a bias introduced by the circle reconstruction.

3.2 Calorimeter-seeded pattern recognition

The calorimeter-seeded pattern recognition starts from grouping the hits in clusters before starting the helix search, but in this case, the calorimeter information (time and position) is driving the process. A calorimeter cluster with the reconstructed energy above 50 MeV identifies a group of hits in the tracker with: (i) a time gate of ±40 ns around the calorimeter cluster time and (ii) a geometrical selection that includes only the hits laying in the same semi-plane identified by the calorimeter cluster in the XY transverse plane. Figure 6 illustrates how the calo-selection works on a typical event with a CE overlaid with the expected background.

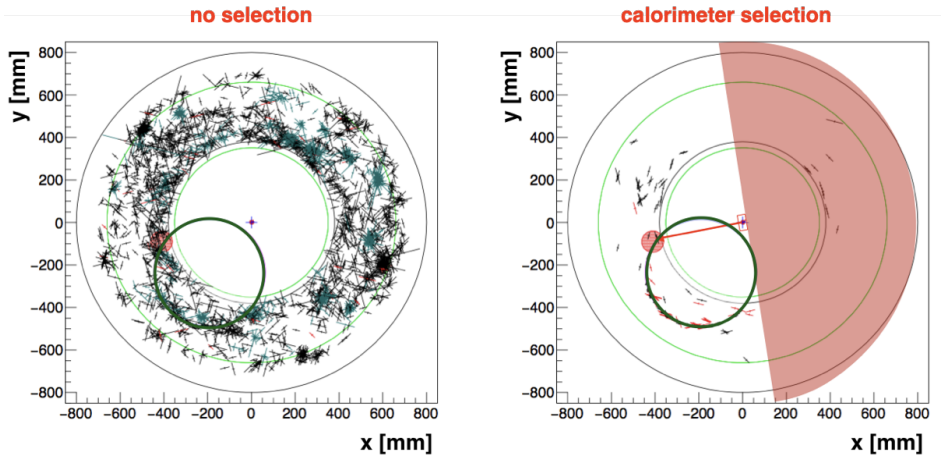

Figure 6: Event display in the XY transverse plane of a typical CE event w/o any selection (left) and after applying the calorimeter selection (right). The black crosses represent the straw hits, the red circle the calorimeter cluster and the green circle the trajectory of the CE.

In this case, the helix reconstruction implements a 3D search. It starts by selecting a triplet with: the calorimeter cluster position, one hit (starting from the one closer to the Stopping Target) and the solenoid center (in the XY plane). A helix defined by these three points determines the initial search-road. Then we loop over all the hits and we pick only one hit per tracking face if it falls within the search road. As soon as the second hit is found, the solenoid center is dropped, and the helix parameters are updated and the procedure re-starts. The algorithm adjusts the helix parameters as the search progresses and new hits are added to the helix candidate. The helix parameters are updated using two different reduced-χ^2 fits: in the XY and the ϕ-Z planes. Each hit is weighted by using the inverse of the square of the expected uncertainty. The hit error is evaluated by projecting its uncertainties (along the wire and radial directions) on the $\vec{r}_{helix}$ and $\vec{\phi}_{helix}$ directions for the XY and ϕ-Z fits respectively. This step is rather important as it allows to take into account the geometrical orientation of the straw tubes w.r.t. to the helix. Figure 7 shows the distributions of the reconstructed momentum and the momentum resolution. The distributions were obtained by processing a dataset of CE overlaid with the expected background sources. A Gaussian fit to the distribution of the momentum residuals shows that the resolution for a CE is $\sim$ 3%. We notice that in this case the mean of the Gaussian fit is at the level of $\sim$0.5 MeV/c, which is a factor $\sim$10 smaller than the previous case. Additional details can be found on this reference[6].

3.3 Track reconstruction

After a helix corresponding to a track candidate is found, a simplified Kalman fit is performed to improve the accuracy in the reconstructed track parameters and thus - the background rejection. This fit doesn't resolve the left-right ambiguity of the hits, nor applies any correction to take into account the energy loss by the particle along the trajectory. Figure 8 shows the distributions of the reconstructed momentum and the momentum resolution. The Gaussian fit to the distribution of the momentum residuals shows that the

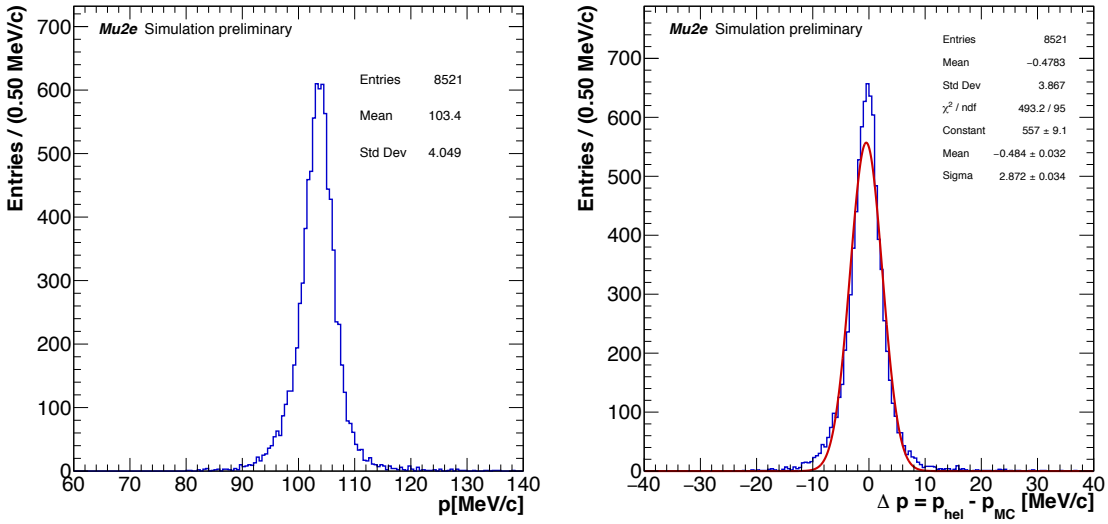

Figure 7: Distribution of the reconstructed momentum (left) and of the momentum resolution (right) for the calorimeter-seeded algorithm. Results were obtained processing a MC sample of CE overlaid with the expected background.

resolution is about 1.4 MeV/c for the CE, which is about two times better than the momentum resolution after the pattern recognition.

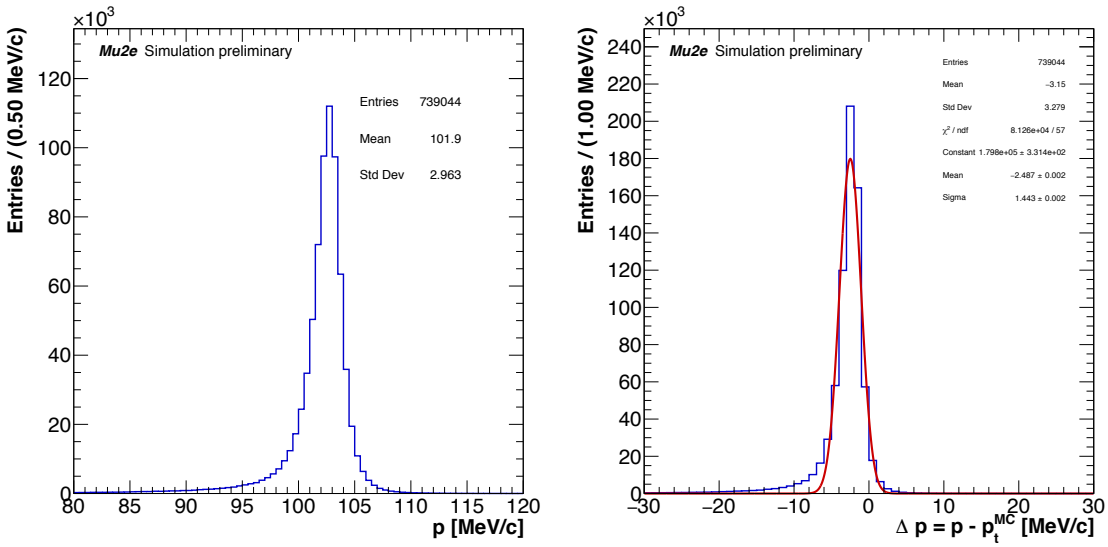

Figure 8: Distribution of the reconstructed momentum (left) and of the momentum resolution (right) for the track reconstruction. Results were obtained processing a MC sample of CE overlaid with the expected background.

4 Expected track-trigger performance

The Mu2e Track trigger is implemented by applying a series of software filters after each step of the track reconstruction. These filters are set up with different settings and the *artdaq*[9] architecture allows to apply

all of them w/o running the reconstruction modules multiple times in the same event. This is especially important for minimizing the running time of the online processing. The expected performance of the track triggers was estimated w.r.t. the offline track reconstruction. In the case of the CE, the resulting efficiency is ∼98% for the OR of the two algorithms, while it's ∼87% or ∼90% if we consider only the calorimeter-seeded or the tracker-seeded algorithm respectively. In the case of the Conversion Positron, the resulting efficiency is ∼96% for the OR of the two algorithms, while it's ∼76% or ∼90% if we consider only the calo-seeded or the tracker-seeded respectively. A lower efficiency of the calorimeter-seeded algorithm for positrons is due to the inefficiency of the online calorimeter clustering algorithm. Figure 9 shows on the left the table with the breakdown of the expected track-trigger rates, while on the distribution of the rejection as a function of the proton bunch intensity (PBI). The total instantaneous trigger rate is expected to be ∼700 Hz; we note that this number is dominated by low-momentum e^- from the Stopping Target and that it can be reduced considerably (either with a pre-scaler or by increasing the momentum threshold) w/o affecting the expected signal trigger efficiency. The same figure shows that the expected total rejection ranges from 2,000 to 500 when PBI/ $<$ PBI $>$ $\in [1, 2]$.

	Instantaneous rate [Hz]
Fakes (tracks mis-reconstructed)	<20
DIO e- from the Stopping Target	680
DIO e- from the inner proton absorber	[~0, 6x10³]
Total	~700

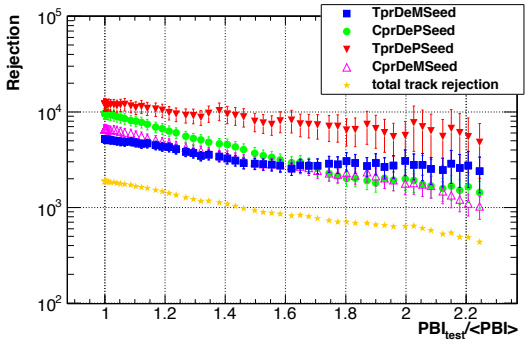

Figure 9: Table with the breakdown of expected track-trigger rates (left) and distribution of expected trigger rejection as a function of the PBI/ $<$ PBI $>$. In the legend, "Tpr" and "Cpr" refers respectively to the tracker-seeded and the calo-seeded algorithms, while "DeM" and "DeP" to downstream electron (Conversion Electron case) and downstream positron (Conversion Positron case).

We performed preliminary tests using the TDAQ test-stand that has been set up at Fermilab. A web-based GUI, powered by the "off-the-shelves" software[7], was used to conduct all the tests. Figure 10 shows the results of the preliminary timing tests that were performed. These results show that the requirement in the total-processing-time is mathed only in the case where one event-builder/DAQ-server is run, while in case of 20 event-builders the time goes up to ∼6.5 ms. We are still in the development stage and several possible solutions to mitigate this issue are being explored.

5 Conclusions

We presented the track trigger system of the Mu2e experiment at Fermilab. The software triggger runs two online pattern recognition algorithms: a tracker-seeded and a calorimeter-seeded algorithm. The expected momentum resolution of both helix search methods is in the range $[3, 4]$% for CE, which is improved by a factor ∼2 by the fast Kalman fit. The resulting trigger efficiency for both CLFV signals Mu2e will be searching is above 96% w.r.t. to the offline reconstruction, while the expected background rejection is ∼2,000 at nominal beam condition. The instantaneous track trigger rate is expected to be ∼700 Hz. This number is dominated by the electrons from the in-orbit decays of captured muons, which can be reduced considerably w/o affecting the trigger efficiency for the signal processes. The preliminary timing tests that we performed with the TDAQ prototype at Fermilab are encouraging, but they also show that improvements are needed to match the requirement of 5 ms/event.

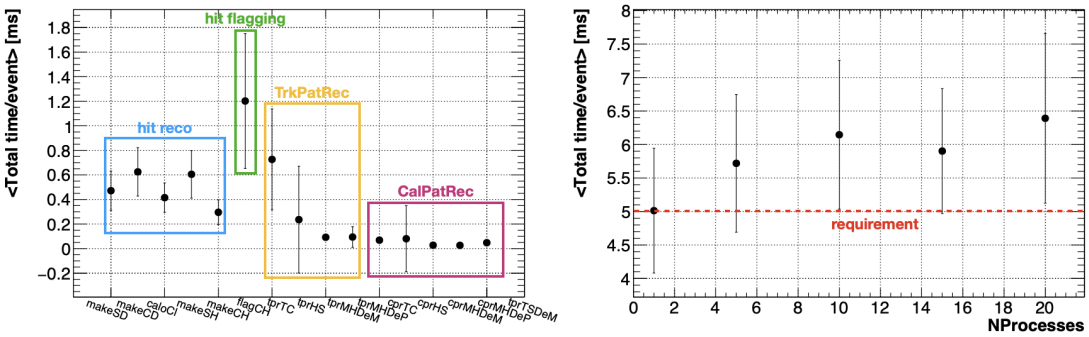

Figure 10: Distribution of the time/event spent by each of the reconstruction module used in the online track reconstruction (left) and of the total reconstruction time/event as a function of the number of event-builder run over the same DAQ server. The box labeled with "TrkPatRec" identifies the modules specific to the tracker-seeded algorithm, while the one labeled with "CalPatRec" the modules referring to the calo-seeded algorithm.

ACKNOWLEDGEMENTS

We are grateful for the vital contributions of the Fermilab staff and the technical staff of the participating institutions. This work was supported by the US Department of Energy; the Istituto Nazionale di Fisica Nucleare, Italy; the Science and Technology Facilities Council, UK; the Ministry of Education and Science, Russian Federation; the National Science Foundation, USA; the Thousand Talents Plan, China; the Helmholtz Association, Germany; and the EU Horizon 2020 Research and Innovation Program under the Marie Sklodowska-Curie Grant Agreement No.690385 and No.734303. This document was prepared by members of the Mu2e Collaboration using the resources of the Fermi National Accelerator Laboratory (Fermilab), a U.S. Department of Energy, Office of Science, HEP User Facility. Fermilab is managed by Fermi Research Alliance, LLC (FRA), acting under Contract No. DE-AC02-07CH11359.

References

[1] Bernstein, Robert H. *et al*, Charged Lepton Flavor Violation: An Experimenter's Guide, Phys. Rep., 532, 2, 27-64, 2013

[2] Bertl, W. *et al*, A search for μ- e conversion in muonic gold, EPJ C, 47, 337346, 2006

[3] Kaulard, J. *et al*, Improved limit on the branching ratio of $\mu^- \to e^+$ conversion on titanium , Phys. Let. B, 422, 334-338, 1998

[4] Bartoszek, L. *et al*, Mu2e Technical Design Report, arXiv: 1501.05241 [physics.ins-det], 2014

[5] Pezzullo, G., The Mu2e Tracker, 39th International Conference on High Energy Physics, FERMILAB-CONF-18-660-E, 2018

[6] Pezzullo, G. and Murat, P., The calorimeter-seeded track reconstruction for the Mu2e experiment at Fermilab, 2015 IEEE Nuclear Science Symposium and Medical Imaging Conference (NSS/MIC), 1-3, 2015

[7] "Off-The-Shelves" web page (last visited 2020-05-15): https://otsdaq.fnal.gov

[8] "The art Event processing framework", web page (last visited 2020-05-15): https://art.fnal.gov/

[9] Biery, K. *et al*, artdaq: An event filtering framework for Fermilab experiment, 18th Real-Time Conference, FERMILAB-CONF-12-278-CD, DOI:10.1109/RTC.2012.6418358, 2012